FEEDBACK CONTROLLED COLLOIDAL ASSEMBLY

WITH USING ANISOTROPIC ELECTRIC FIELD

by

Junyan Yang

A thesis submitted to Johns Hopkins University in conformity with the requirements for the degree of Master of Science in Engineering

Baltimore, Maryland

April 2019

ABSTRACT

Feedback Controlled Colloidal Assembly

with Using Anisotropic Electric Field (Apr, 2019)

Junyan Yang, B.E., Tianjin University, China

Chair of advisory committee: Dr. Michael A. Bevan

The goal of this study is to explore the use of anisotropic electric field to facilitate colloidal silica particle into quasi two-dimensional defect-free big colloid domain in high yield and efficiency. The anisotropic electric field introduced here is generated by octupole electrode, which has eight identical electrodes pointing to the center. It can be fabricated through a series of photolithography and metal deposition. Using electric field to tune colloid assembly has been continuously investigated for years, however, applying anisotropic electric field to programmable control colloid assembly process has not yet been studied. In comparison with precedent work, we introduce newly designed control policies combine with isotropic and anisotropic electric field to enhance the performance on assembling colloidal particles into perfect crystal.

Two types of anisotropic electric field with different orientation were introduced in this work, they are coupled with isotropic electric field to obtain perfect crystal structure. Grain boundary in colloid ensemble can be expected to be relaxed through morphology change between electric fields. An image analysis function was developed to assist colloid assembly process. It enables program to analyze real-time status of current system, and

report certain order parameters including crystallinity, grain boundary orientation to represent the state of colloid ensemble.

Open-loop and closed-loop control policies were also developed to realize programable control function. Open-loop control policy enables colloid ensemble experience periodical change between two types of anisotropic field with isotropic electric field applied between each anisotropic field period. Closed-loop policy relies on the grain boundary orientation feedback to the program to determine the ideal anisotropic electric field applied on next period to relax grain boundary.

These two control policies coupled with anisotropic electric field exhibits significant improvement on yield of perfect crystal and efficiency. We also empirically optimize the update time, which is the duration of each type of electric field applied, from 50 seconds to 20 seconds to further shorten the total time cost. It shows great progress on improving colloid assembly efficiency while maintain high success rate. This work demonstrates the use of anisotropic electric field and control policies on enhancing performance of colloid assembly.

Committee: Prof. Michael A. Bevan (academic advisor, ChemBE)

Prof. Joelle Frechette (ChemBE)

To my dear parents and family members

ACKNOWLEDGEMENTS

First, I would like to thank everyone who is being supportive to me through all the way from a child to an adult. Especially my dear parents, who have been supportive on every decision I made on study and allow me to purse my dream in abroad. Also, my family members, thank you for giving me happiness and motivate me to be a better person.

I'd like to thank Dr. Michael A. Bevan, for being such a great academic advisor. Thank you for giving me support on research projects and graduate school application. You are truly the role model in academia. Your kindness, mentorship shaped me to the researcher that I am today, gave me instructions on performing research and building future career.

I'm grateful for my incredible lab members, Isaac, Helya, Nikki, Jianli, Jenny, Rachel, Zhaonian, Yuanxing and Lechuan. It's my honor to work with you, thank you for helping me on experiments, bringing laugh to our office, making every day easy and happy and showing me what a good graduate student should be. Also, for the past group members, Xiaoqing, Matt and Ramona, thank you for sharing all joyful moments with me, I wish you all the best in your career.

A special thank you to my mentor, Jianli, thanks for teaching me all the experimental skills, master student life from all aspects and being such a good friend to me.

I'm grateful for all my friends in Johns Hopkins University, my friends in China, especially Hongjie and Daoning, our friendship make me through every tough moment, thank you for experiencing the best time of life with me together.

TABLE OF CONTENTS

LIST OF TABLES

LIST OF FIGURES

1. INTRODUCTION

1.1Background

Colloid is a mixture in which one substance of microscopically dispersed insoluble particles is suspended throughout another substance[1]. Usually, it can be classified into eight categories based on the dispersed phase and disperse medium, including liquid aerosol, emulsion, gel, etc*. Colloid suspension possesses huge importance in daily life and industries. Colloids are usually seen in paints, milk, and cream in daily life, while in photonics[2], ceramics[3], drug formulation[4], raw oil[5], chemical sensors in industries[6]. Recent progress on studying colloid science focus on formation of low defect and single domain colloid crystal for applications in photonic materials[7], nano-optical coatings and devices[8], templates for porous materials[9], catalysis[10], and even in biomedical engineering field.

Previous nanoscale patterning uses top-down method[11], however, it requires elaborate facilities and only permits two-dimensional structure design[12]. Current art and science of colloid crystal formation usually relies on self-assembly, a process by which individual components arrange themselves into an ordered structure. Self-assembly can be approached by evaporation of solvent[13], gravitational confinement[14], depletion force[15], field restraints[16], temperature control[17], etc.

Colloid assembly exhibit significant importance in various applications, including drug delivery system, pharmaceutical processing, dairy industries, oil refinery, etc[18]. The main challenge in current colloid assembly study is to produce large single domain colloid crystal with high efficiency. Numerous methods have demonstrated their capacity to successfully assemble colloidal particles[19-22]. However, some of them are not able to

produce reversible and controllable assembly, making it harder to fix multidomain and dislocations. Applying electric field, as one of the novel approaches, shows great potential to tune colloid assembly process and correct defects[23-26].

Colloid assembly using external electric field has been investigated for years. Different types of colloidal particles including chiral particles[27], janus particles[28], polymer particles[29], cubes[30], etc. were fabricated into various sets of colloidal structures. Many research groups reported to use DC or/and AC field to direct the assembly structure from one-dimensional colloid chains, two-dimensional arrays, to three-dimensional clusters[31-32]. Two-dimensional colloid structure is of vital importance for its use as mask of nanosphere lithography, templates for photonic materials and metamaterials[33].

In previous studies reported from our lab, quadrupole which has four identical electrodes pointing to the center was designed to generate isotropic electric field to tune colloid assembly process[26, 34]. The colloidal particle ensemble was periodically relaxed and assembled, so that grain boundary in colloid array may be relaxed. This method provides new way to assemble particles into defect-free colloidal crystal. Here, we aim to develop new type of electrode, electric field and control policies to further improve the colloid assembly process.

1.2 Objective

The main objective of this study is to investigate the use of isotropic and/or anisotropic electric field in colloid assembly, test and modify control policies on obtaining colloid crystal in short time with high efficiency. Colloidal sized silica particles are used in experiments, as the properties of silica particles are well defined, and the modification

and functionalization of silica particles is relatively easy. Isotropic electric field was studied by previous members in lab, the properties and characteristics are well understood[35]. Anisotropic electric field is newly proposed to facilitate colloid assembly process based on previous investigation on electric field.

The first goal of this work is to design and fabricate suitable electrodes which can provide both isotropic and anisotropic electric field. We proposed to design octagonal electrodes, which can be referred as 'octupole', where eight separate identical electrodes are equidistantly placed, and pointing to the same center. Octupole electrodes are fabricated through photolithography and e-beam, similar as the process that our lab developed before*.

The second goal of this work is using newly designed electrodes to generate isotropic field and/or anisotropic field to control colloid assembly process. Four types of control policies are designed through previous experience to improve colloid assembly performance. Control policies are executed through experiments and modified based on results. Under each control policies, colloidal particles experience different electric field in different sequence. We hope they are able to provide a practical and convenient way to obtain large single domain, defect-free colloid crystal in short time.

1.3 Essay outline

This essay is organized into five separate chapters to report research progress in colloid assembly from different aspects. Chapter 1 describes the significance and background of research project, gives rough description about the reason and perspective on investigating current art and science of colloid assembly by using electric field.

Chapter 2 elucidates the theory of electric field assisted colloidal particle assembly, including particle-particle interaction, particle-field interaction, etc. Basic principles and formulas are provided to help understand colloidal particle electric properties and colloid assembly mechanism in electric field.

Chapter 3 provides methods on experimental parts. Octupole electrodes are fabricated through photolithography and followed by e-beam gold evaporation coating. Experiment samples are set up on the surface of obtained octupole by loading certain amount of micron sized silica particle. Video microscopy, function generator, and computer are connected. Order parameters are introduced to quantify colloidal particle system and configuration. A series of tool box are developed on MATLAB platform and improved based on previous experiment methods. They are used to control experiments, track and analyze colloidal particle movement, at the meanwhile, providing real-time calculation results of certain order parameter to define current system. Several control policies are developed to control colloid assembly process by tuning electric field frequency and/or magnitude. Certain control policies can 'smartly' control assembly process based on real-time feedbacked parameters. Obtaining single domain perfect crystal is the ultimate goal for experimental part.

Chapter 4 presents detailed explanation of experimental results from each different control policies. Experiment results are summarized and compared with simulation results to verify the accuracy of experiment execution, also giving insights on understanding colloid assembly process in electric field.

Chapter 5 summarizes results from different control policies, brings out potential methods to enhance programmable colloidal particle assembly in anisotropic electric field

based on previous experiment results. Future directions on investigating colloid assembly through electric field assistance are elucidated.

2. THEORY

2.1 Interaction and Potentials

2.1.1 Net Particle Interaction

The net particle interaction of concentrated colloidal particle in a non-uniform electric field consists of three parts, the particle-particle interaction, the particle-wall interaction, and the particle-field interaction. It is given by,

$$u^{net} = u^{pp} + u^{pw} + u^{pf} \tag{1}$$

2.1.2 Particle Interaction on Direction Perpendicular to The Substrate

Particle interaction on direction perpendicular to the substrate consists of two parts, the gravitational potential energy on particle, and the particle-wall interaction only includes electrostatic repulsion when Van der Waals interaction is negligible[36]. It is given by,

$$u^{vertical} = u_g^{pf}(z) + u^{pw}(z) \tag{2}$$

where the first term represents the gravitational potential energy, and it is given by,

$$u_g^{pf}(z) = Gz \tag{3}$$

$$G = \frac{4}{3}\pi a^3(\rho_p - \rho_m)g \tag{4}$$

where $G=4/3\pi a^3(\rho_p - \rho_m)g$ is the buoyant particle weight, ρ_p and ρ_m are the particle and medium densities, and g is acceleration of gravity.

The second term in Eqn.2 represents the particle-wall interaction when Van der Waals interaction is negligible, it is given by,

$$u^{pw}(h) = u_e^{pw}(h) \tag{5}$$

And $u_e^{pw}(h)$ is given by,

$$u_e^{pw}(z) = B^{pw} \exp[-\kappa(z-a)] \tag{6}$$

$$B^{pw} = 64\pi\varepsilon_m a\left(\frac{kT}{z_v e}\right)^2 \tanh\left(\frac{z_v e\psi_p}{4kT}\right)\tanh\left(\frac{z_v e\psi_w}{4kT}\right) \tag{7}$$

where ψ_p and ψ_w are the particle and wall stern potentials, and h is the particle-wall surface-to-surface separation, Z_v is the electrolyte valence.

2.1.3 Particle Interaction on Direction Parallel to The Substrate

The particle interaction on direction parallel to the substrate consists of three parts, the electrostatic interaction due to the static surface charge, and particle-particle potential due to applied electric field, and particle-field interaction, it is given by,

$$u^{horizontal} = u_e^{pp}(r_{ij}) + u_{dd}^{pp}(r_{ij}, \theta_{ij}, x, z) + u_{de}^{pf}(R) \tag{8}$$

The first term in Eqn.8 represents the electrostatic interaction for thin electric double layers ($\kappa a \gg 1$), it is given by[37],

$$u_e^{pp}(r_{ij}) = B^{pp} \exp[-\kappa(r_{ij} - 2a)] \tag{9}$$

Where r_{ij} is the particle-particle distance between random particle i and j, a is the particle radius, κ is the Debye length, and B^{pp} is the pre-factor for pair electrostatic repulsion between particles, it is given by,

$$B^{pp} = 32\pi\varepsilon_m a\left(\frac{kT}{e}\right)^2 \tanh^2\left(\frac{e\psi_p}{4kT}\right) \tag{10}$$

where ε_m is the medium dielectric constant, k is Boltzmann's constant, T is absolute temperature (in Kelvin), e is the charge of an electron, ψ_p is the particle Stern potential.

The second term in Eqn.8 is the particle-particle potential due to applied electric field, it can also be referred as induced-induced dipole interaction, it is given by[38],

$$u_{dd}^{pp}(r_{ij}, \theta ij, x, z) = -kT\lambda f_{\phi} P_2(\cos\theta_{ij})(2a / r_{ij})^3 E^*(x,z)^2 \tag{11}$$

where θ_{ij} is angle between the line connecting particle centers and the electric field line direction, $P_2(\cos\theta_{ij})$ is the second Legendre polynomial, $E^*(x,z)$ is the local normalized electric field and it is equal to $E(x,z)/E_0$, and λ non-dimensional amplitude, given as[38],

$$\lambda = \pi\varepsilon_m a^3 (f_{cm} E_0)^2 / kT \tag{12}$$

In here, f_{cm} is the Clausius-Mosotti factor given as,

$$f_{cm} = \mathrm{Re}[(\tilde{} \quad \tilde{} \quad \tilde{} \quad \tilde{} \tag{13}$$

where $\tilde{\varepsilon}_m$ and $\tilde{\varepsilon}_p$ are the complex medium and particle permittivities of the form $\tilde{\varepsilon} = \varepsilon - (i\sigma/\omega)$, where σ is the conductivity and ω is the angular frequency. The particle conductivity is given as $\sigma = 2K_n/a$, where K_n is the surface conductance[39].

The third term in Eqn.8 represents the induced dipole interaction within electric field. It is given by[40],

$$u_{de}^{pf}(R) = -2kT\lambda f_{\phi} f_{cm}^{-1} E^*(R)^2 \tag{14}$$

where $f_{\phi} f_{cm}$ is the volume fraction, and $E^*(R)$ is the electric field in the central portion of octupole electrode.

2.2 Order Parameter

Order parameters were introduced to calculate the status of current colloidal system. They were also known as reaction coordinates in previous research and reports from our group. The Order parameters reflect the state of system, including the colloidal array structure, space density, etc. to help us understand colloid assembly. There are three order parameters are of major interest, the global six-fold bond orientational order, six-fold connectivity, and grain boundary orientation.

2.2.1 Global Six-fold Bond Orientational Order

The global six-fold bond orientational order represents the degree of crystallinity of current system. It is given by[41-42],

$$\psi_6 = \left| \frac{1}{N} \sum_{j=1}^{N} \psi_{6,j} \right| \tag{15}$$

Where N is the total number of particles in the ensemble, j is the particle number, and $\psi_{6,j}$ is the local six-fold bond orientation order of particle j given as[43],

$$\psi_{6,j} = \frac{1}{N_{C,j}} \sum_{k=1}^{N_{C,j}} e^{i6\theta_{j,k}} \tag{16}$$

where $N_{C,j}$ is the number of neighbor particles within the first *g(r)* peak (coordination radius) of particle *j*, and $\theta_{j,k}$ is the angle between particle *j* and each neighbor particle *k* with an arbitrary reference direction by connecting the center of particle *j* and particle *k*.

2.2.2 Six-fold Connectivity

The six-fold connectivity represents the degree of close-packed structure of current system. It is calculated from the local six-fold connectivity by checking the connectivity between crystalline particles. The connectivity is formulated as[44],

$$\chi_{6,jk} = \frac{\left|\mathrm{Re}[\psi_{6,j}\psi^{*}_{6,k}]\right|}{\left|\psi_{6,j}\psi^{*}_{6,k}\right|} \tag{17}$$

where $\psi_{6,j}$ is the complex conjugate of $\psi_{6,j}$. By checking connectivity between crystalline particles, we can obtain local six-fold connectivity, $C_{6,\,j}$, which is an integer range from 0 to 6. The local six-fold connectivity is given by[45],

$$C_{6,j} = \sum_{k=1}^{N_{C,j}} \left[\begin{vmatrix} 1 & \chi_{6,jk} \geq 0.32 \\ 0 & \chi_{6,jk} < 0.32 \end{vmatrix} \right] \tag{18}$$

Thus, the global six-fold bond connectivity C_6 can be obtained by averaging local six-fold bond connectivity, then normalized by the C_6 value of 2-dimensional hexagonal close-packed particle with hexagonal morphology.

$$C_6 = \frac{1}{N}\sum_{i=1}^{N} C_{6,i} \Big/ \langle C_6 \rangle_{HEX} \tag{19}$$

Where $<C_6>_{HEX}$ represents the C_6 value of limited area of close-packed particle array. In infinite area of close-packed particle array, the C_6 value should be 1.

3. Materials & Methods

3.1 Electrode Fabrication

3.1.1 Slide Preparation

Thin gold film octupole electrodes were patterned through photolithography and metal deposition processes. The microscope cover glass coverslip (Corning) were put into sonication with acetone for 30 minutes, then followed by sonication with iso-propanol for another 30 minutes. Cleaned cover glasses were dried using high purity nitrogen, then cleaned by using Nochromix glass cleaning solution for 20 minutes. Cover glasses were rinsed with deionized water and dried out with nitrogen. They were kept in isopropanol to avoid contamination from environment.

3.1.2 Spin Coating

A thin sacrifice layer is introduced on the top of clean cover glass before photolithography. Prior to spin coating, clean slides are dried with nitrogen and heated on hot plate which was set 200℃ for 5 minutes. Heated slides were cooled down to room temperature and put into spin coating machine. The spin coating parameters are set as spinning speed: 3000 rpm, duration: 60s, acceleration: 150 rpm/s. Slides were covered with S1813 (Shipley) before starting of spin coating. After spin coating, slides were cross-linked on 95℃ hot plate for 5 minutes.

3.1.3 Exposure and Development

Slides were put into photolithography machine for patterning. The exposure energy should be set from 80 mJ/cm^2 to 100 mJ/cm^2 for clear pattern of electrode shape. Electrode

mask were put above the slide before starting. Exposed slides were merged into CD26 solution for development, followed by rinsing with deionized water. Moderate shaking was applied for faster development and cleaning. Condition of pattern was examined under microscope to ensure accurate patterning of electrodes.

3.1.4 Metal Deposition

Slides were attached to the cap of Sharon vacuum before loading programs of e-beam machine. After reaching ideal vacuum condition automatically set by the program for metal deposition, chrome was first evaporated to cross-link with glass with a rate of 0.2 A/s. 25nm thickness of chrome layer was desired. Gold was then evaporated to cross-link with chrome layer deposited in the same deposition rate. 15nm thickness of gold layer was ideal for octupole fabrication. After metal deposition, the inner pressure of Sharon vacuum was released, slides were taken out and sonicated with iso-propanol until octupole pattern was clear and accurate. Octupole were dried with nitrogen and heated on 95℃ hot plate for 5 minutes for further cross-linking. They are cooled down to room temperature and kept in iso-propanol before using.

3.2 Preparation Techniques

3.2.1 Particle Purification

3.13 μm diameter silica particles were used for assembly experiments. However, the polydispersity of silica particles bought from industries could lead to severe dislocation in colloid assembly experiment. Therefore, silica colloids were purified before using through gravitational sedimentation to select particles with identical (roughly similar) size, as sedimentation speed is direct correlated with particle volume. 1 mL as-received stock

silica particles were added to 33 mL DI water in clean glass test tube #1, then sealed glass tube with parafilm to avoid contamination. Colloid suspension was vigorously shaken for 1 minutes by Vortex Genie machine then sonicated for 5 minutes to fully disperse and suspend colloidal particles. When sedimentation line approached half of the total volume line, 1 mL of sedimented silica dispersion was removed using glass Pasteur pipette approximately one third of the distance from the top of the colloidal sedimentation line. 1 mL DI water was added to tube #1 to keep total volume of dispersion fixed. The removed silica dispersion was added to clean glass test tube #2 with 33 mL DI water. Repeating same procedures as described above, 1 mL removed silica dispersion was added into clean glass test tube #3 for storage. 10 μL of purified silica dispersion was put on clean microscope slide and examined under Inverted Microscopy. Silica dispersion from tube #3 can be used for experimental use only if major parts of particles shows unique size through microscopy observation. If not, repeat sedimentation process described above until silica colloids with identical size were obtained.

3.2.2 Particle Suspension Making

Colloid assembly using electric field can reach a high efficiency while in DI water system, reported by previous research progress from our lab. To toughen up our case, DI water was replaced by 0.1 mM salt solution, as the Debye length of silica particle in salt solution is decreased, the movement between particles are much more difficult, lead to a tougher case for fixing grain boundary for colloid assembly. 4.0 mg NaOH was weighed by electronic balance then dissolved in 100 mL volumetric flask with 100 mL DI water. 1 mL of purified silica dispersion was added into 2 mL centrifuge tube and allowed to fully sedimented by gravitational force for 3 hours. Supernatant fluid was removed with glass

Pasteur pipette and replaced by 1 mL made 0.1 mM NaOH solution. New colloidal suspension was agitated through Vortex Genie machine for 1 minutes and sonicated for 5 minutes.

3.2.3 Function Generator Connection

Agilent dual channel function generator 33500B was connected to computer to enable programmable control of colloid assembly process. The driver of Agilent function generator was installed to computer before using. Insert the Agilent disk into the CD drive and install the Agilent I/O library. When installation is complete, insert the USB cable and navigate to the CD drive with the Windows Driver Wizard. Windows should now recognize the Agilent function generator as a valid USB device. MATLAB is used for manually automatically control function generator through codes.

Accessing Agilent dual channel function generator 33500B could be implemented by MATLAB command as follow: inst = visa('agilent','USB0::0x0957::0x2C07::MY52805062::0::INSTR'). This whole command can be interpreted as accessing Agilent through its device specific IP address. The first term in ‘visa’ command is identifying dual channel function generator as ‘Agilent’ instrument. The other term is for finding and connecting certain instrument, which is Agilent function generator in here.

3.2.4 Camera Connection

High resolution camera was required for capturing images and/or videos to record and analyze colloidal particle assembly process, understand movement and status of each

particles. Several parameters for connecting camera with computer through MATLAB command can be found as follow,

```
DEVICE = 'hamamatsu';
FORMAT = 'MONO8_BIN4x4_336x256';
camera = videoinput(DEVICE,1,FORMAT);
set(camera,'ReturnedColorSpace','gray');
triggerconfig(camera,'Manual');
camera.TriggerRepeat = Inf;
camera.FramesPerTrigger = 1;
src = getselectedsource(camera);
src.ExposureTime = 1/100;
start(camera)
```

The first command is for accessing device driver specific for ‘Hamamatsu Camera’. The second command is for setting resolution of captured image (336 pixels * 256 pixels) and camera binning was set as 4. (camera binning can be varied as 1, 2, 4, 8, and they correspond to different resolution) the third command is for load camera with defined format input video. The forth command is for returning grayscale only images as they are easier for realizing several future image analysis functions, including particle tracking, etc. The fifth command is for realizing capturing images until stopped manually or by program. The sixth command is for realizing capturing 560 frames per trigger. The eighth command made the camera exposure for every 0.02s. After running commands above, camera parameters were all set, and it should be able to capture images or record videos as expected. In real cases, experiment processes were saved as ‘tif’ files by camera capturing function. The ‘tif’ files can be translated into ‘avi’ files through ‘ImageJ’ program.

Also, Streampix can be used to capture videos without using MATLAB and executing command above. After setup connection between Streampix and camera following instruction on Streampix manual, videos of colloidal particle movement could be recorded. Resolution, frame rate per second, bin number, frames needed per film, etc. can be specified in settings before video capturing. The recorded video comes with 'seq' format, and it can be translated into 'tif', 'avi' and 'mp4' formats using its internal translation function, and further analyzed with other methods. Streampix is primarily used for early stage experiments for understanding particle movement, anisotropic electric field characteristics and examining new control methods.

3.2.5 Microscope Setup

Inverted microscope was required for revealing movement of colloidal particles in assembly experiments. Zeiss Axio Observer A1 inverted microscope was placed on the horizontal table near computer to avoid any fluctuation that could influence the accuracy of experiments from machine and other instruments. Inverted microscope was connected to 'Hamamatsu' camera, and the camera was connected to the computer. The microscope was set with 63× objective without magnification unless otherwise stated. Level meter was used to ensure inverted microscope was at the horizontal level, as any inclination of microscope would undermine the forces colloidal particles are experiencing on horizontal level. There was a knob near each table leg, they can be used for tuning the height of table, to keep horizontal table from inclination.

3.2.6 Sample Preparation

Colloidal particle assembly experiment samples are made by following procedures. Octupole electrodes were sonicated in acetone for 45 minutes, then sonicated in iso-propanol for another 45 minutes. The electrodes were dried with nitrogen gas and rinsed into Nochromix glass cleaning solution for 20 minutes, followed by rinsing with DI water and dried with nitrogen. Clean octupole electrodes were interfaced with copper wires for connection to Agilent dual channel function generator.

4 pairs (8 in total) of short copper wires with similar length (3-4 inches) were cut with scissors. The copper wires came with red color insulation wrap which can keep from short circuit. The insulation wrap was shaved off about half inches at both ends of the wire by using small razor blade. Each copper wire was interfaced with each separate electrode by using the conductive carbon tape. Conductive carbon tape was cut into small squares (0.25 - 0.5 inches). Shaved end of copper wire was laid rest above electrode then covered with small piece of carbon tape. Peeled off the cover of carbon tape, use tweezer to press on the carbon tape to ensure good adhesion between carbon tape, electrode and copper wire. Same procedure was performed to all other separate electrodes. The free end of copper wires from opposite side on octupole electrodes were manually attached together to ensure both conductive parts were tightly engaged. Also, check with the copper wires and ensure no shaved part were in contact with others to keep short circuit from happening.

A 1 cm diameter O-ring was covered with vacuum grease on both sides then put onto the center of octupole electrodes. Using tweezer to press on the O-ring to make sure it was firmly contact with substrate below. Free ends of copper wires were connected to function generator through the cramp of cable connected with function generator.

3.2.7 Sample and Equipment Setup

After finishing ensemble batch cell sample, it was transferred to microscopic room. Turn on Zeiss Axio Observer A1 inverted microscope. Turn objective to 63×, and magnitude to 1× respectively. Put sample onto sample stage and using clips on the stage to fix sample's location. 4 pairs of copper wires were categorized into two groups, the pairs that were attached to neighbor electrodes were the same group. Connect any pair of wires in Group 1 to Channel 1 ground line of function generator output by using the clamp at the end of connection wire. Connect another pair of wires in Group 1 to Channel 1 active line of function generator output. In Group 2, the pair of wires which attached to the Group 1 active line neighbor electrode was connected with Channel 2 ground line, and the last pair of wires was connected with Channel 2 active line. The order of copper wire connection with function generator output is extremely important for generating the right anisotropic electric field. Check the connection between clamps and the copper wire to avoid loose connection. Also, check the peeled parts of copper wires, make sure no peeled parts were in contact with others to avoid short circuit. Then, turn on function generator.

40 μL 0.1 mM NaOH solution was added onto the top of octupole electrode center inside of the O-ring. Wait for 5 minutes to stabilize the electric charge distribution on the top surface of electrode and glass. Then, 40 μL colloidal silica suspension was added into NaOH solution after sonication for 5 minutes. Allow silica particle to sediment and form single layer on top of electrode for 5 minutes. At the meantime, adjust lamp knob to get proper brightness for sample observance. Tune coaxial coarse and fine focus knobs to focus on silica particle layer to have clear image of particle movement.

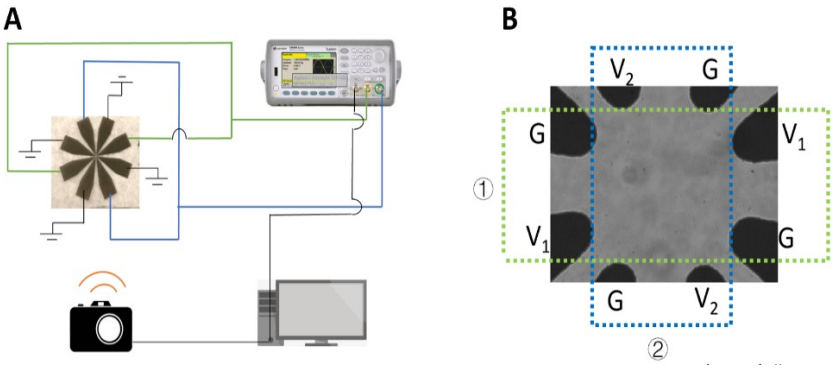

Fig 3.1 (A) sketch of connection of devices. Octupole electrodes is connected to the dual channel function generator Agilent 33500B through the order stated. The function generator is connected to the computer, it can be accessed and controlled by the computer program. The high-resolution CCD camera placed underneath the electrode and align with the octupole center. The CCD camera is connected to the computer, to enable video capturing and feedback images to computer for analysis. (B) The microscope image of center of the octupole electrode. The electrodes are categorized into two pairs as shown in blue box and green box. In here, G is denoted as the electrodes connected to the ground line, V is denoted as the electrodes connected to the active line. Electrodes pair 1 are connected to channel 1 of function generator, while pair 2 are connected to channel 2.

3.3 Image Analysis

3.3.1 Video Capturing

'Load_Parameters' is a preconfigured function that contains a series of experimental parameters including assembly time, objective, $\psi_{6\text{scale}}$, etc. to facilitate video capturing and order parameters calculation.

The '[inst, camera] = Connect_Devices(opt_device)' command realizes function to connect 'hamamatsu' camera and Agilent dual channel function generator 33500B with computer simultaneously. After running second command, the MATLAB software should be able to execute commands to control function generator output with determined frequency and voltage.

The 'preview(camera)' command transferred real-time image/video output to MATLAB platform. It shows a clear image with a 334×256 resolution.

3.3.2 Particle Tracking

Particle tracking function was realized by distinguishing the greyscale of particles and background. Under the inverted microscope, silica particles were reflected with white color, and the background was grey. Image every frame was automatically put into multiple 1×1 pixel square, the light squares exceed greyscale cutoff threshold (usually 45 or 60) were identified as light square. The light square which has six light square neighbors was determined as the center of silica particle, thus each particle that meets the greyscale requirement was found and labeled as particles need to track. Also, the particles away from other particles were classified as isolated particles, and they will be filtered to not be counted into particles actively been used in current system. The particle tracking command consists of three parts.

The first part of particle tracking function was designed to filter certain particles which meet the greyscale threshold requirement and point out their geometry center. The particle center could be used to generate particle coordinates to help calculation of order parameters.

The second part enabled MATLAB to remove colloidal particles which are 20 pixels away from the nearest particles. In experiments, particles will be quenched into the center of electrodes, and form colloid array with certain shape corresponds to the electric field. However, some particles may drift around the array or stuck on the edge of electrodes. These particles are away from the colloid array and should not be counted when calculate order parameter of current system.

The third part formulated output particle number data.

3.3.3 Grain Boundary Identification

After applying certain electric field, the particles were quenched into the center of electrodes, a close-packed array was formed. If a single domain colloid array is formed, there should be no visible grain boundary seen under the inverted microscope, and this array could be identified as perfect crystal. If multiple domains were formed, there should be at least one grain boundary inside of current system, and it needs to be identified through MATLAB system for further analysis.

Particle coordinates were obtained from Image Analysis toolbox in MATLAB, the local order parameters $C_{6,i}$, and $\psi_{6,i}$ were calculated based on Eqn.16, 17, 18. For particles which have $C_{6,i}$ <0.7, they are identified as peripheral particles, which can be seemed as particles locate on the peripheral layer of the entire colloid array. For particles satisfy $C_{6,i}$>0.7 and $\psi_{6,i}$<0.95 requirement, they are identified as 'grain boundary particles', which can be understood as particles locate on the grain boundary, or on the edge of particle domains. For particles which have $C_{6,i}$>0.7 and ψ_6 >0.95, they are identified as 'crystalline particles', which can be understood as particles located inside of big colloid domain. Through comparing the values of local order parameter, grain boundary can be found.

3.3.4 Real Time Status Update

The purpose of status update is to provide thorough information for observation and documentation of experiments. The variables displayed and documented in status update includes current number of experiment cycle, the time of current cycle spent, control option, number of particles, global six-fold bond orientational order, global six-fold connectivity, gyration, grain boundary orientation and number of successful cycles. This

information will be documented in the ‘OP_data’ in txt format, also be displayed in the MATLAB command window.

Also, image of current cycle will be documented in 1 frame/s in ‘tif’ format. The particle coordinates and order parameters will be documented every second in ‘txt’ format.

3.3.5 Color Scheme

Color scheme provides a thorough method for visualizing order parameter and status of experiments. Each particle will be dyed in to different colors based on the order parameters. The particles will be first identified as useful particles by particle tracking functions. Then, calculate global order parameters, and local order parameters for each particle based on method stated above.

From we stated in section 3.3.4, the grain boundary particles, crystalline particles, peripheral particles were identified by comparing the local order parameters of each particle. If two or more grain boundary exist in current system, the major grain boundary is distinguished by comparing the particle numbers of each grain boundary. The major grain boundary is colored with yellow color, while the minor grain boundary is colored in different color.

For other particles, they will be dyed into different shades of blue, based on the local order parameter $C_{6,i}$ of each individual particle. They will also be dyed into a single scale of red based on the global order parameter ψ_6. The final color of colloid array combines these two types color scheme together, while grain boundary particles remain yellow color.

For grain boundary particles, a line which across the mass center of grain boundary particles is plotted at the center of grain boundary, to indicate the location of grain boundary for easy identification in experiment review.

3.4 Electric Field

3.4.1 Isotropic Field Introduction

Isotropic electric field was first introduced into colloidal assembly experiment in previous studies reported by our lab in using quadrupoles. The quadrupole provides an isotropic field, which has uniformity in all orientations. The isotropic electric field can be obtained by applying single channel voltage to electrodes. Octupole is also able to generate isotropic field by applying same voltage on both channels. The isotropic electric field can be used for quenching particles and relax previous colloidal array structures. Fig 3.2 shows isotropic electric field generated by quadrupole and octupole.

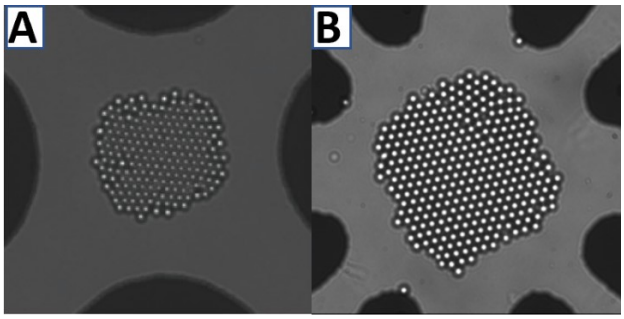

Fig 3.2 the structure of colloid ensemble structure corresponds to the electric field applied to the system, thus allow us to use colloid array shape to represents the shape of electric field. (A) colloidal particle array in isotropic field generated by quadrupole. (B) colloidal particle array in isotropic field generated by octupole.

3.4.2 Anisotropic Field Introduction

Anisotropic electric field is introduced into colloidal assembly experiment for very first time. It can be interpreted as electric field with anisotropy in every direction. In simulation and experiments, it shows an oval shape with respect of the ratio of voltage applied on each pair of electrodes of octupole. For obtaining the most elliptical shape of anisotropic electric field, the voltage applied to pair 1 of electrodes to pair 2 equals to 5:2. In previous experiments, we demonstrated that a high total voltage applied on octupole would lead to multi-layer structure of colloid ensemble, and a total voltage of two pairs equal to 2.7 V can avoid the multi-layer problem, while facilitate colloid assembly in best extent. So, in here, 1.93V and 0.77V are applied to octupole. Octupole was categorized into two pairs of electrodes in Fig 3.1 B. Fig 3.3 shows two types of anisotropic electric field by applying 1.93V to pair 1 and 0.77V to pair 2. Fig shows 0.77V to pair 1 and 1.93V to pair 2. Based on absolute lab coordinate, the field orientation in Fig 3.3A is defined as $\beta_1 = 112.5°$, the field orientation in Fig 3.3B is defined as $\beta_2 = 22.5°$.

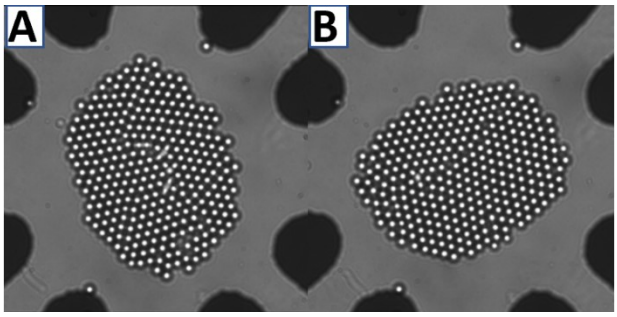

Fig 3.3 using structure of colloid ensemble to represent shape of anisotropic electric field applied. (A) anisotropic electric field with 1.93V applied on pair 1, and 0.77V applied on pair 2. (B) anisotropic electric field with 0.77V applied on pair 1, and 1.93V applied on pair 2.

Anisotropic field provides a series of various conditions of electric fields that previous experiments never have. We hope the morphology change between anisotropic

and isotropic fields could induce the merge of colloidal domains, relaxation of grain boundary, contribute to helping particle arrays reach perfect crystal state with a high success rate and shorter time cost.

3.5 Control Policies

3.5.1 Constant Control

Control policy is the major composite of colloid assembly experiment. By tuning the control policy, we can have various combinations of different electric fields. The change between electric fields will induce the change of grain boundary, thus helping colloid array reach perfect crystal state.

The first control policy we use in experiment is the constant control policy. It was designed to examine the success rate of colloid assembly in isotropic electric field in nature.

After setting up with function generator and high-resolution camera, a constant electric field with 1.35 V and 1 MHz on both channels were actuated for 500 seconds. Particles quickly moved to the center of electrodes under the influence of field-dipole interaction and form a close-packed single layer of colloid array. The array usually consists of two or more particle domains separated by grain boundary. Although the colloid system is currently close-packed, the particles are still able to move in limit space, especially multiple domains may merge into single big domain and reach perfect crystal state. Cycle ends when ψ_6 is higher than 0.90, which can be deemed as perfect crystal state. Cycle also ends when time cost has been greater than 500 seconds.

After finishing each cycle, a weak isotropic field with 0.135V applied on both channels was actuated to relax its current formation, enable particles move freely and back to their initial condition, which is fluid phase.

The constant policy focuses on the capability of fixing grain boundary by single type of isotropic electric field itself. Constant control policy was written in MATLAB command under 'assembly_control' function section. After executing function, the command automatically updates particle numbers, order parameters including ψ_6, C_6, and grain boundary orientation every second, also save these data into txt format, under the name of 'Cycle_cylce number_OP'. The command will also record screenshots of experiment every second and save image into tif format under the name of 'Cycle_cylce number'. Particle coordinates will also be saved into txt format under the name of 'Cycle_cycle number_CO'. These files could be used for further analysis and experiments review.

3.5.2 Open-loop Isotropic Policy

Open-loop isotropic policy was also tested in previous experiments using quadrupole. Here, open-loop policy was used to examine the efficacy and success rate on octupole.

Open-loop isotropic policy consists of two types of isotropic field. The electric field was alternating between high voltage isotropic field, which was also called 'isotropic - quench field' and low voltage isotropic field, which was also called 'isotropic – relax field'. The isotropic - quench field was actuated by applying 1.35 V on both channels, and isotropic – relax field was actuated by applying 0.135 V on both channels. The former one enables particles get together and form a close-packed colloid array, the later one enables

colloid array relaxing its current formation, allows particles moving freely in a weak electric field confinement, also keeps particles from escaping from the center of octupole.

In experiments, the assembly test started from fluid phase, where particles are randomly distributed above the octupole slide. Two types of isotropic fields were alternating applied every 50 seconds (update time), with 'isotropic – quench' field applied at first to make particles form initial colloid array structure. In every stage that applied with 'isotropic – relax' field, particles slowly dissociate from close-packed structure to fluid phase, grain boundary was also relaxed. Then, in next stage with 'isotropic – quench' field applied, particles back to close-packed structure again from fluid phase, form multi-domain structure with new grain boundary, or directly form a perfect crystal. Cycle ends when ψ_6 is greater than 0.9 or time cost is over 500 seconds. The statistics and experimental images are saved in the same format in same way described in constant policy section. The policy flow sheet can be found below.

Open-loop isotropic policy allows particles to move in a small distance, and usually enables most particles have different neighbor particles after 50 seconds of relaxation, thus allow the shift, remove of grain boundary and merge of multiple colloid domains. This policy provides solution for cycles of experiment that cannot be fixed by applying only constant field itself to resolve grain boundary.

3.5.3 Open-loop Anisotropic Policy

Open-loop anisotropic policy was introduced into colloid assembly experiment for first time. The anisotropic field generated by octupole provides two types of electric field with different orientations, which can be combined using with isotropic electric fields. The transformation of electric field, no matter from circular shape isotropic field to oval shape

anisotropic field, or from anisotropic to isotropic field, even between two types of anisotropic fields will induce the movement of particles and domains. We hope the displacement of particles will lead to shift of grain boundary or even fully removal of grain boundary, and help current system reach perfect crystal state in a shorter time.

The open-loop anisotropic policy consists of four parts. The two types of anisotropic field with different orientations alternating coupled isotropic - quench field between them. First, 1 MHz 1.35V were applied on both channels to make particles quench at the center of octupole for 50 seconds. After stabilizing, 1.93V on channel 1, and 0.77 on channel 2 were applied to octupole and generate anisotropic field for another 50 seconds. Then, isotropic – quench field was applied again to restore the circular shape for another 50 seconds. At last, 0.77 V on channel 1 and 1.93 V on channel 2 were applied to octupole to generate anisotropic field with different orientation than we use in the second 50 seconds slot. Cycle ends when ψ_6 is greater than 0.9 or time spent is over 500 seconds.

In the first stage, particles moved from randomly distributed fluid phase to the center of octupole under field-dipole interaction and form circular shape single layer colloid array. Then, in second stage, colloid array gradually changed to oval shape corresponds to the anisotropic electric field, the orientation of particle cluster also aligns with anisotropic field orientation. The grain boundary shifts as the array was stretched on long axis, squeezed on short axis of anisotropic field. In the third stage, particle array restored its circular shape under isotropic field, the grain boundary newly formed under this condition exhibits different location or/and different orientation than the one in the first stage. In the fourth stage, particle array gradually changed to oval shape with different

orientation than in the second stage under the influence of anisotropic field, particles movements and grain boundary shift were observed.

The transformation of colloid cluster induced by alternating between anisotropic and isotropic field leads to anneal of colloid domains, and increase of global order parameter, ψ_6, thus resolve grain boundary, and lead current system to perfect crystal state in a fast manner.

3.5.4 Closed-loop Anisotropic Policy

Closed-loop anisotropic policy was further improved based on open-loop anisotropic policy. It also uses anisotropic and isotropic electric field in the experiment to help colloid array reach perfect crystal state faster. The aim of developing closed-loop policy is to determine suitable anisotropic field with desired orientation based on certain parameters in experiment to help fix grain boundary, and minimize the time spent on applying opposite anisotropic field. In here, grain boundary orientation was taken into consideration, as simulation results shows there is strong connection between anisotropic field orientation and grain boundary orientation for fixing grain boundary.

We define grain boundary orientation $\alpha = \min [| \gamma - \beta_1 |, | \gamma - \beta_2 |]$, and γ is defined as the orientation of grain boundary based on the absolute lab coordinate, and it ranges from -90° to 90°. The grain boundary orientation at here represents the minimum value of angle between grain boundary and the orientation of each type of anisotropic fields.

The anisotropic field type I shown in Fig 3.3A was defined with orientation $\beta_1 = 112.5°$, and anisotropic field type II shown in Fig 3.3B was defined with orientation $\beta_2 = 22.5°$.

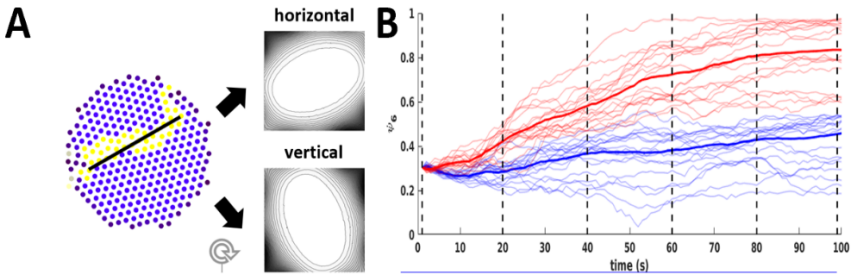

Fig 3.4 anisotropic electric field with different orientation applied to same initial state of colloid ensemble. The ψ_6 value was monitored through whole process. (A)initial colloid ensemble with specified grain boundary orientation, to be applied with horizontal anisotropic electric field and vertical anisotropic electric field separately. (B) The change of ψ_6 value as a function of time after applied with each anisotropic electric field. Applied with horizontal electric field (red line); applied with vertical electric field (blue line).

Fig 3.4 shows simulation works of anisotropic electric field decision making process. All cycles of experiment start from a low ψ_6 value, which is 0.4, and has orientation of grain boundary $\gamma = 22.5°$ as shown above. Two types of anisotropic field were each applied for this condition for several cycles. The global order parameter ψ_6 was monitored for whole simulation process. Plot ψ_6 value - time for each cycle and both types of anisotropic field.

As Fig 3.4 shows, under this condition, most cases that applied with anisotropic field orientation $\beta_2 = 22.5°$ lead to increase of ψ_6, and many of them reach the perfect crystal state, which is $\psi_6 = 0.9$. However, most cases that applied with anisotropic field orientation $\beta_1 = 112.5°$ shows vulnerability on improving ψ_6.

The results can be concluded as, if $| \gamma - \beta_2 | < 45°$, then anisotropic field with orientation $\beta_2 = 112.5°$ will be better for improving ψ_6. If $| \gamma - \beta_1 | < 45°$, then anisotropic

field with orientation $\beta_1 = 22.5°$ will be better for improving ψ_6. Same simulations were carried out for other initial conditions with different grain boundary orientations. The results were similar and matched with the conclusion described above. To be simple, always choose the field orientation that is closer to the grain boundary orientation for improving ψ_6. The measurement of deciding anisotropic field applied to system was also called ‘decision making’ or ‘anisotropic field choosing’.

Based on that, closed-loop policy enables MATLAB program to choose ideal anisotropic field for relaxing grain boundary and improve ψ_6 in every anisotropic field section. The closed-loop policy was also made of four parts, with isotropic – quench field applied between every anisotropic field period. The flowsheet can be found below.

With the help of anisotropic field orientation choosing, the ideal anisotropic field for relaxing grain boundary will always be applied, thus shorten the total time cost, also improve assembly success rate.

4. Results and Discussion

4.1 Results Introduction

Colloid assembly experiments by using different control policies and newly designed anisotropic electric fields enhanced performance on assembling silica colloidal particles into perfect crystal structure in high efficiency.

The preparation of sample slide, pairs of electrodes are connected to the dual channel function generator following the Fig 3.1A. The order of connecting function generator is important to the experiment, especially on generating the right type of electric field.

The material system consists of 300 3μm silica colloidal particles dispersed in 0.1 mM NaOH solution. Initially, the system was not applied with electric field, and Van der Waals interaction is negligible, the only external field effecting system is gravitational field. Particles are uniformly under the influence of gravitational force, thus maintain a quasi-2-dimensional pattern above the surface with a random particle distribution due to Brownian motion.

After applying electric field, electrostatic interaction and gravitational interaction remain the same. The inhomogeneous electric field induced dipoles interact with each other also with the spatially inhomogeneous electric field, known as the induced dipole-induced dipole interaction and particle-field interaction.

In previous research from our group, induced dipoles experience the minimum potential energy at the minimum electric field energy, which locates at the center of

octupole electrodes under high frequency electric field. Particles respond to this effect and move to the center of octupole. This phenomenon is referred as 'field-dipole interaction'.

In low frequency electric field, induced dipoles experience the minimum potential energy at the minimum electric field energy located at the edge of octupole electrodes. Particles respond to the electric field and move into the electrodes away from the octupole center. Under these mechanisms, we can tune colloid assembly process by changing electric field.

4.2 Colloid Assembly Results with Different Control Policies

4.2.1 Constant policy Results

Constant policy was executed to examine to capability for fixing grain boundary, obtaining single domain colloid array solely by constant isotropic electric field itself. The experiment starts from fluid phase, where particles are randomly distributed above the slide. The only external field for system is gravitational potential field that confines the particles in a quasi 2-dimensional configuration. We examine the yield of perfect crystal, median time cost and average time cost for obtaining perfect crystal structure in 100 cycles of experiments. Here, the average and median time cost is defined as the average and median value of time for all cycles that finished with perfect crystal structure, failed cycles are not taken into consideration. Cycle ends when ψ_6 reach 0.90 or time cost is over 500s.

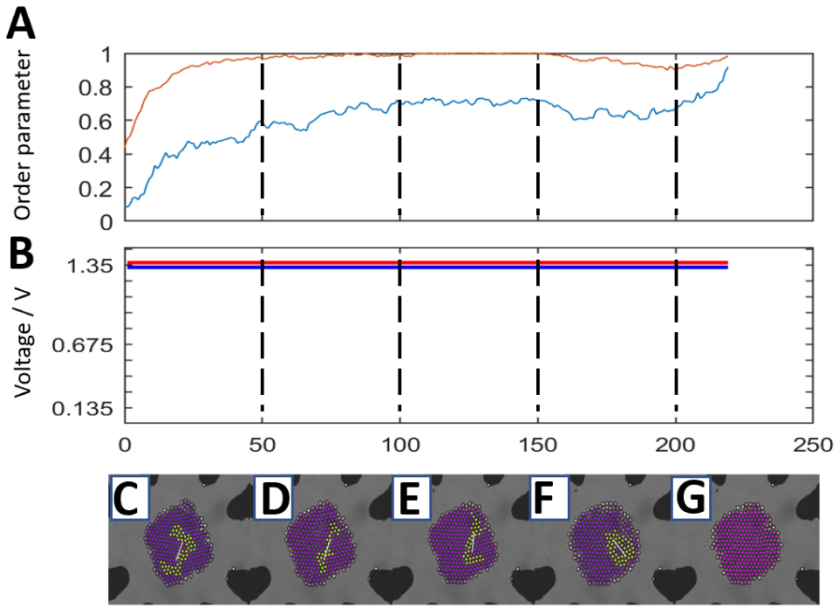

Fig 4.1 Single trajectories of selected cycle from constant control policy experiment. The isotropic quench field which has 1.35V on both channels is applied. (A) Order parameters for individual cycle, global six-fold bond orientational order, ψ_6, (blue line); six-fold bond connectivity, C_6, (red line). (B) Trajectories of voltage applied on each pair of electrodes. voltage applied on channel 1 (blue line), voltage applied on channel 2 (red line). (C-G) Representative snapshots from the experiment images.

From the data we obtained, 62% of experiments cycles were able to finish at perfect crystal state, however, there are still 38% of cycles are not able to finish with defect-free single domain colloid configuration. At here, the average time is 254s, while the median time cost is 151s. These results show limited cycle of experiments can end up with perfect crystal structure and it usually costs a relatively long time as the relaxation of grain boundary purely relies on the hindered Brownian motion of particles.

Fig 4.1A shows order parameters of selected experiment cycle, grain boundary orientation is plotted in dash line as it is not contributed to the constant policy control. The ψ_6 value remain around 0.6 for a while, it indicates the system reached a plateau of ψ_6 after forming close-packed colloid array. Fig 4.1C-G shows a series of snapshots of selected

experiment cycle. At early stage, the limited Brownian motion was not able to produce major effects on relaxing grain boundary, particles at the center of array were kept immobile, only particles at periphery are able to move around the boundary of entire system. Grain boundary was not relaxed until the particles at the edge of different domains started to move, ψ_6 was significantly increased and the system quickly reached the perfect crystal state.

However, not all cycles that finished with perfect crystal structure can relax grain boundary within short time, half of successful cycles require a time over 200s to fix grain boundary by solely applying isotropic quench field itself.

4.2.2 Open-loop Isotropic Policy Results

Open-loop isotropic policy was investigated and reported on using quadrupole in previous works from our lab. Here, we examine the open-loop isotropic policy on octupole electrodes. It enables colloidal particles relax its configuration after forming multiple domain colloid array through applying weak isotropic electric field to enable less limited hindered Brownian motion.

The open-loop isotropic policy utilizes weak isotropic field to relax grain boundary. The alternating isotropic – quench and isotropic – relax field allows cycles that cannot finish with perfect crystal structure by only applying isotropic – quench field opportunity to re-ensemble by relaxing its current configuration. Two types of isotropic electric fields alternate every update time (here, update time = 50s), start with isotropic - quench field at first. Cycle ends when ψ_6 reaches 0.90, which can be seemed as perfect crystal, or time cost is over 500s. Experiments were repeated for 100 cycles.

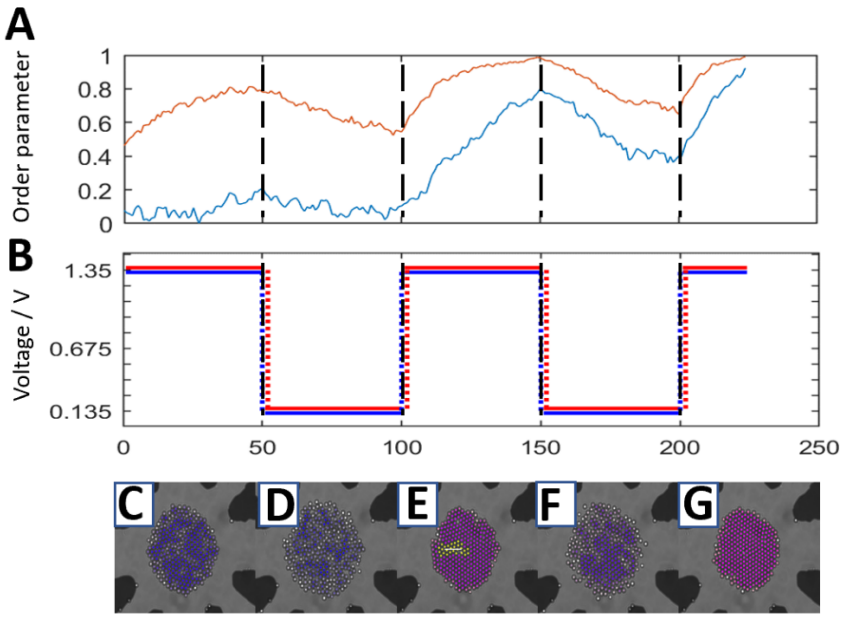

Fig 4.2 Single trajectories of selected cycle from constant open loop isotropic policy experiment. The isotropic quench and isotropic relax field are alternatingly applied to the octupole. (A) Order parameters for individual cycle, global six-fold bond orientational order, ψ_6, (blue line); six-fold bond connectivity, C_6, (red line). (B) Trajectories of voltage applied on each pair of electrodes. voltage applied on channel 1 (blue line), voltage applied on channel 2 (red line). (C-G) Representative snapshots from the experiment images.

From the data we obtained, yield of perfect crystal, average and median time cost were calculated. The success rate exhibits significant improvement compared with constant policy. 80% of cycles from experiments finished with perfect crystal structure. The open-loop isotropic policy shows capability on fixing grain boundary in a better way, while didn't show major impact on accelerating assembly process.

ψ_6 and C_6 from selected trajectory are plotted as a function of time are shown in Fig 4.2A. ψ_6 kept in low value in the first update time. In second update time, ψ_6 value was decreased as the relaxation of ensemble. In third update time, ψ_6 value greatly increased as relaxation of ensemble also realized the relaxation of previous grain boundary, thus enabled formation of a minor grain boundary in the third update time. In the fourth update time, ψ_6

decreased for relaxation of ensemble, and reach the perfect crystal state at the fifth update time. The trend of C_6 also corresponds to the periodic change of electric field.

Fig 4.2C-G shows screenshots from selected trajectory of experiment cycle. A new grain boundary with smaller impact on overall particle uniformity was produced after relaxing previous ensemble in second update time. A defect-free single domain colloidal array was obtained after relaxation in forth update time. The open-loop isotropic policy provides method on improving success rate of colloid assembly experiment, while didn't show great promise on shortening the time cost at the same time.

4.2.3 Open-loop Anisotropic Policy

We took advantage of the anisotropic field that octupole can generate and combine with isotropic electric field to further enhance control policy to better tune the colloid assembly process. The two types of anisotropic field with different orientation is the key that leads to morphology change of colloid array. In open-loop anisotropic policy, grain boundary is relaxed by the periodic morphology change of ensemble.

The open-loop anisotropic policy consists of four parts, with isotropic electric field applied between alternating anisotropic fields with different orientations. At each stage, certain electric field was applied for update time (here, update time = 50s). In each anisotropic field stage, grain boundary was stretched in the direction aligned with current anisotropic field orientation and squeezed at its perpendicular direction. In isotropic electric field stage, the colloid array restored circular shape and form a new grain boundary. Cycles ends when ψ_6 reaches 0.90, which can be seemed as perfect crystal structure, or time spent is greater than 500s. Experiments were repeated for 100 cycles.

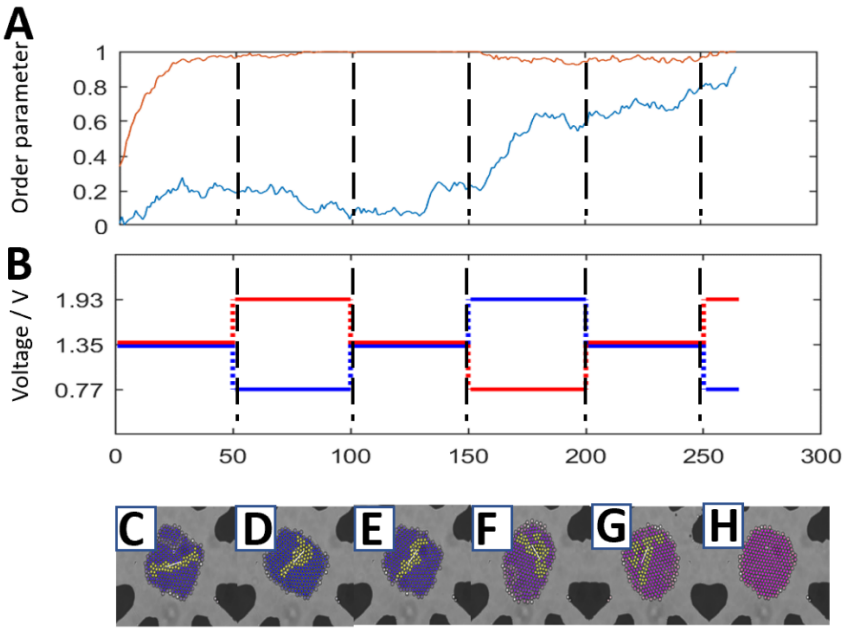

Fig 4.3 Single trajectories of selected cycle from open loop anisotropic control policy experiment. The isotropic quench field was applied between two types of anisotropic field period, each electric field was applied for 50s. (A) Order parameters for individual cycle, global six-fold bond orientational order, ψ_6 , (blue line); six-fold bond connectivity, C_6, (red line). (B) Trajectories of voltage applied on each pair of electrodes. voltage applied on channel 1 (blue line), voltage applied on channel 2 (red line). (C-H) Representative snapshots from the experiment images.

From data we obtained, yield of perfect crystal, average and median time cost were calculated. The success rate exhibits improvement compared to the first two control policies stated. 98% of cycles successfully finished with perfect crystal structure. The average and median time cost significantly drops to 141 s and 112s. With the help of anisotropic field, grain boundary can be fixed by the morphology change between different electric fields rather than the stochastic process of ensemble relaxation in open-loop isotropic policy, thus, assembly can be finished with an efficient manner.

Selected cycle of experiments is represented. ψ_6 and C_6 are plotted as a function of time in Fig 4.3A. In the fourth update time period, grain boundary was relaxed at its greatest

extent, where exhibits significant increase of ψ_6 value. After applying anisotropic field, in the fifth update time period, the isotropic electric field quench particles into circular shape, then system quickly reach perfect crystal structure.

Fig 4.3C-H represents a series of screenshots from the selected trajectory of experiment. The colloid array transformed from circular shape to oval shape in second update time period. Although ψ_6 doesn't exhibit increasing during this period, several domains were merged into two separate big domains which will be an asset for expediting assembly process in next step. In the fourth update time period, colloid array transforms into oval shape with orientation vertical to the one in second update time period, allows the increase of ψ_6 value for entire system. The open-loop anisotropic policy shows capability on improve perfect crystal yield while shortening time cost.

4.2.4 Closed-loop Anisotropic Policy

Closed-loop anisotropic policy was developed based on open-loop anisotropic policy. The closed-loop policy enables program controllable choosing ideal type of anisotropic field to relax grain boundary. The right choice on applying anisotropic field should result in further improvement on perfect crystal yield and efficiency.

The closed-loop policy consists of two parts, the isotropic – quench field and anisotropic field with determined orientation via program feedback. The assembly control always starts with applying isotropic – quench field at first. The update time at here is 50s. From decision making simulation results shown in Fig 3.4, we can see the anisotropic field with orientation with smaller angle between field orientation and grain boundary is preferred for relaxation of grain boundary. Based on this, grain boundary orientation is set as the feedback parameter to determine the suitable orientation of anisotropic field applied

on next step. Status including order parameters are updated every second, the last ten grain boundary orientation value in each period applied with isotropic field will be averaged to ensure the accuracy of feedback control. Experiment is repeated for 100 cycles, cycle ends when ψ_6 is greater than 0.90, which is high enough to deem current system as perfect crystal or time cost is over 500s.

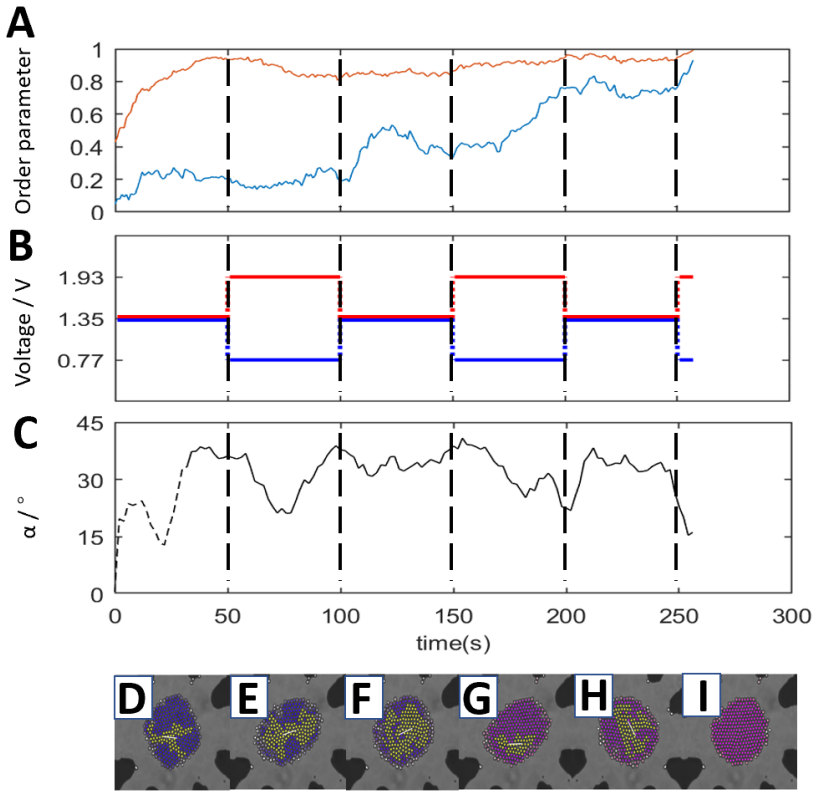

Fig 4.4 Single trajectories of selected cycle from closed-loop anisotropic control policy experiment. The isotropic quench field was applied between each determined anisotropic field period, each electric field was applied for 50s. (A) Order parameters for individual cycle, global six-fold bond orientational order, ψ_6 (blue line); six-fold bond connectivity, C_6 (red line). (B) Trajectories of voltage applied on each pair of electrodes. voltage applied on channel 1 (red line), voltage applied on channel 2 (blue line), grain boundary orientation in current system (black line). (C) Grain boundary orientation, α, as a function of time. (D-I) Representative snapshots from the experiment images.

From the data we obtained from experiments, the yield of perfect crystal, average and median time cost were calculated. The yield of perfect crystal reaches 100%, it validates the feasibility and accuracy of closed-loop decision making mechanism. The average time cost is 160s, which is a bit higher than the open-loop anisotropic policy, while the median time cost remains the same as 112s. The closed-loop policy doesn't show significant improvement on time cost for obtaining perfect crystal. However, it helps for solving certain cases that open-loop policy is not capable to fix, and helps the yield of perfect crystal reach 100%.

Selected cycle of experiments is represented. ψ_6 and C_6 are plotted as a function of time as in Fig 4.4A. In Fig 4.4C, grain boundary orientation was plotted in dash line when C_6 is lower than 0.9, where no accurate grain boundary orientation can be obtained. Grain boundary orientation was plotted in solid line after C_6 reaches 0.9. From Fig 4.4A, In the second update time, the determined anisotropic field relax grain boundary and helps increase ψ_6 value in small extent. In the fourth update time, the determined anisotropic field relax grain boundary in large extent and ψ_6 value exhibits great increase. The closed-loop anisotropic policy enables the ψ_6 to increase at whole process, making the assembly process easier to finish with perfect crystal structure, while the open-loop policy cannot.

Fig 4.4D-I represents a series of screenshots from the selected trajectory of experiment. We can see anisotropic field with same orientation was applied in second and forth update time period, and they both contribute to the increase of ψ_6 value in some degree. The closed-loop policy provides a programmable policy that can smartly choose ideal condition based on current status of system, it greatly helps colloid assembly to finish in a high efficiency manner.

4.2.5 Empirical Optimization of Closed-Loop Anisotropic Control Policy

Closed-loop anisotropic policy has achieved superior progress on expediting colloid assembly process in obtaining defect-free perfect crystal structure. We intend to further improve the efficiency of assembly and propose to use smaller update time to further shorten the total time cost. As in empirical, it takes long time for particles reaching dynamic stable state. However, the anisotropic policy proposed in here only requires particle array transform into the morphology that corresponds to the electric field. Thus, the remaining time in each update time after forming electric field corresponding colloid structure can be omitted. Here, 20s is used as new update time to optimize the control policy, also examine the yield of perfect crystal and assembly efficiency on both open-loop and closed-loop policies.

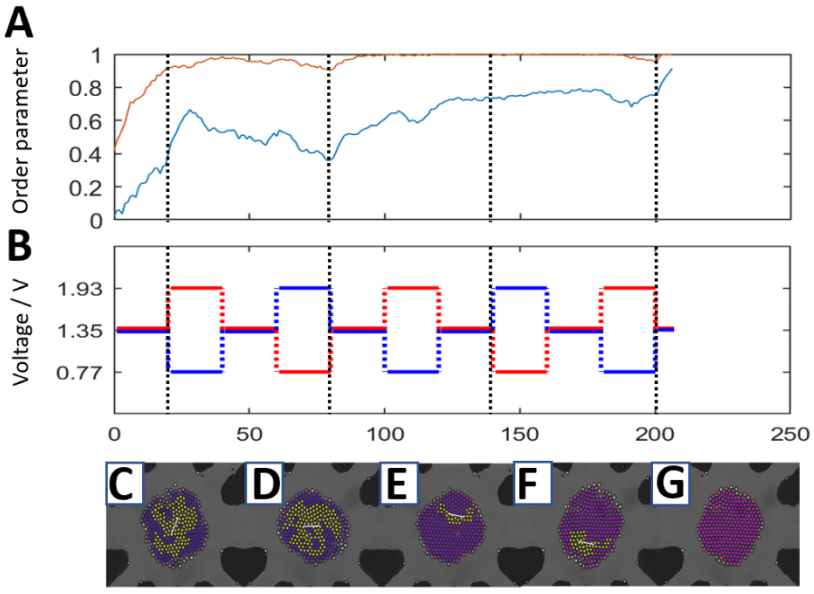

Fig 4.5 Single trajectories of selected cycle from open loop anisotropic control policy experiment. The isotropic quench field was applied between two types of anisotropic field period, each electric field was applied for 20s. (A) Order parameters for individual cycle, global six-fold bond orientational order, ψ_6 , (blue line); six-fold bond connectivity, C_6, (red line). (B) Trajectories of voltage applied on each pair of electrodes. voltage applied on

channel 1 (red line), voltage applied on channel 2 (blue line). (C-G) Representative snapshots from the experiment images. The snapshots in here represents the real-time status of last second image of each interval separated by the black dash line in Fig 4.5A-B.

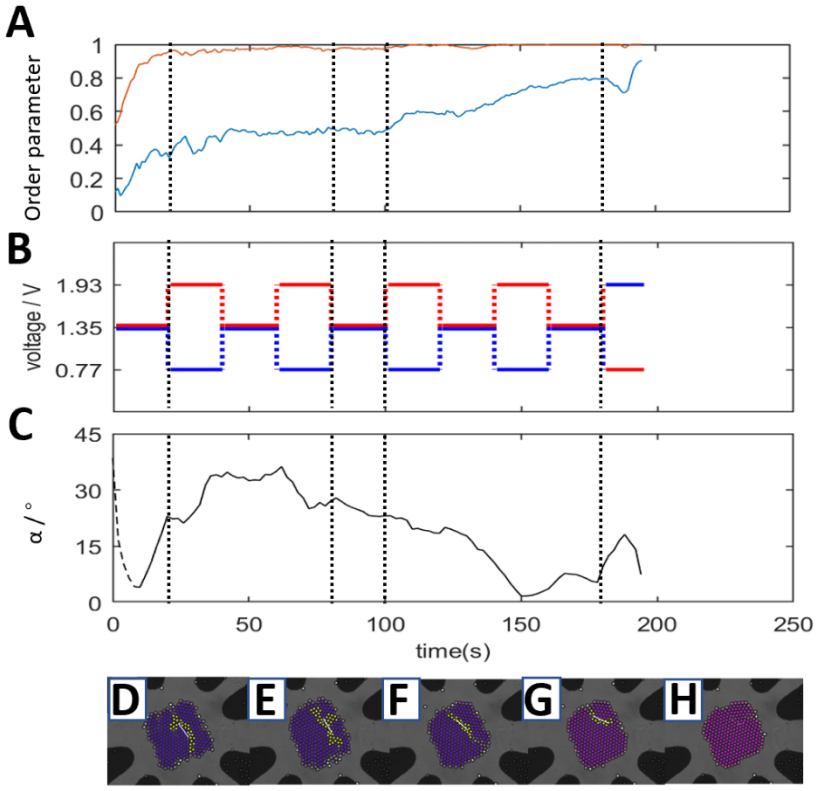

Fig 4.6 Single trajectories of selected cycle from close loop anisotropic control policy experiment. The isotropic quench field was applied between each determined anisotropic field period, each electric field was applied for 20s. (A) Order parameters for individual cycle, global six-fold bond orientational order, ψ_6 , (blue line); six-fold bond connectivity, C_6, (red line). (B) Trajectories of voltage applied on each pair of electrodes. voltage applied on channel 1 (red line), voltage applied on channel 2 (blue line), grain boundary orientation in current system (black line). (C) Grain boundary orientation, α , as a function of time. (D-H) Representative snapshots from the experiment images. The snapshots in here represents the real-time status of last second image of each interval separated by the black dash line in Fig 4.6A-C.

From the data we obtained from experiments, the yield of perfect crystal, average and median time cost were calculated. The average and median time cost both exhibit significant decrease in both policies, it validates previous proposal on using small update time to further shorten total time cost. However, the perfect crystal yield of open-loop

anisotropic policy remains 98%, which means there are certain cases of grain boundary cannot be relaxed by open-loop policy.

Selected cycle of experiments is represented. ψ_6 and C_6 are plotted as a function of time as shown in Fig 4.5A and Fig 4.6A. ψ_6 value exhibits same trend in previous experiments where update time = 50s. The change of update time will not affect the yield of perfect crystal. Smaller update time shows great improvement on time efficiency of colloid assembly process, while maintaining yield of perfect crystal at high level. For open-loop anisotropic policy, the average and median time cost reduced to 92s and 72s, while for closed-loop anisotropic policy, they were shortened to 108s and 60s. Similar experiments were also executed as update time = 40s or 10s. Among these experiments, 20s shows much superior effect on shortening the total time cost, as 40s is still too long for particles reach their field corresponding ensemble structure; 10s is too short for particles fully reach the field corresponding ensemble structure, thus bringing side effect to the experiment. The empirical optimization of experiments provides ideas on shortening colloid assembly time cost. For now, update time = 20s is a safe choice for experiment execution.

4.2.6 Statistical Summary of Control Policies

Here, we summarize the experimental results of different control policies tuned colloid assembly process. Fig 4.7. shows the cumulative success rate distribution from each control policies. The policies involve using anisotropic electric field shows significant improvement on perfect crystal yield compared with policies which only use isotropic electric field. The anisotropic electric field employed in control policies greatly improved the yield of perfect crystal through the morphology change of colloid ensemble.

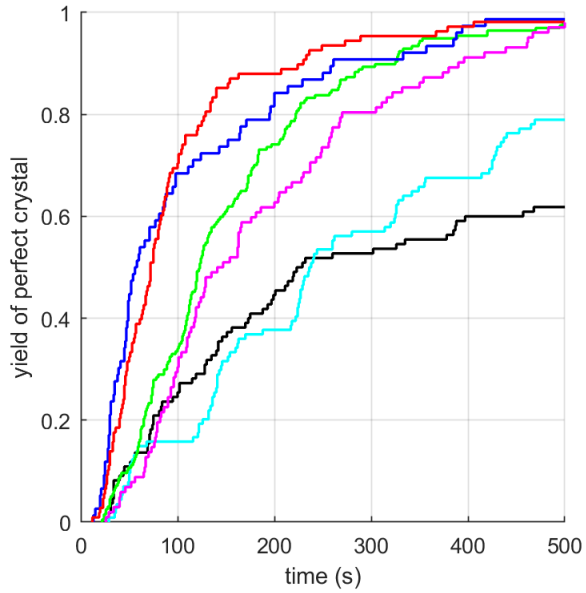

Fig 4.7 the cumulative success rate distribution as a function of time. Constant control policy (black line), open-loop isotropic control policy (light blue line), open-loop anisotropic control policy (green line), closed-loop anisotropic control policy (pink line), open-loop anisotropic control policy with update time = 20s (blue line), closed-loop anisotropic control policy with update time = 20s (red line).

From Table.1, the average and median time cost was both significantly reduced by employing either open-loop and closed-loop policy. By optimize update time from 50s to 20s, the time cost was further decreased, while maintain a high perfect crystal yield. The time cost results between open-loop and closed-loop policy didn't exhibit a great difference, possibly due to the inaccuracy of grain boundary analysis. Despite these flaws, the closed-loop policy provides new method on controlling colloid assembly experiments by feedback certain parameter to program controllably choosing ideal anisotropic electric field to relax grain boundary.

	Const.	OL iso. (50s)	OL aniso. (50s)	CL aniso. (50s)	OL aniso. (20s)	CL aniso. (20s)
yield/%	62	80	98	100	98	100
t_{ave}/s	254	250	141	160	92	108
t_{ave}/s (simulation)	236	256	152	167	98	110
t_{med}/s	151	215	112	112	72	60

Table 1. Statistical results of perfect crystal yield, average and median time cost for successful cycles in experimental work and average time cost in simulation work for all control policies stated.

5. Conclusion and Future Work

5.1 Conclusion

Previous studies reported several methods on assembling colloidal particles including using electric fields. In work reported from our group, isotropic electric field generated from quadrupole electrode shows advanced behavior on ensemble particles into perfect crystal structure. Here, we proposed to develop a new type of electrode, which has eight identical electrode pointing to the center, to facilitate assembling silica colloidal particles into large single domain perfect crystal in short time with high success rate by using electric field.

The octupole electrode is obtained from photolithography and metal deposition patterning. Octupole electrode can generate two types of anisotropic electric field with different orientation which has never been studied in colloid assembly before. We use these newly introduced anisotropic electric field to develop control policies (open-loop and closed-loop policies) to tune colloid assembly process. In both simulation and experiments, they have shown significant progress on facilitating colloid ensemble reaching defect-free colloidal crystal within high yield and efficiency, compared with precedent work. The new policies took advantage of two types of anisotropic field with different orientation to induce the morphology change of colloid array, so that grain boundary can be relaxed during the transformation of electric field.

Several order parameters were introduced into this work, including six-fold bond connectivity C_6, global six-fold bond orientational order ψ_6, and grain boundary orientation α to represent certain status of current ensemble. An image analysis function was

introduced into current system, it enables the program to precisely control the number of particles stay in the system, analyze real-time status of colloid ensemble and feedback accurate information for next-step analysis.

Through decision making simulation, we found the anisotropic field with orientation parallel to the grain boundary will be the best condition for grain boundary relaxation. If the grain boundary is not able to parallel with either field orientation, then the anisotropic field with orientation closer to the grain boundary orientation is the ideal one to be applied into current system. The closed-loop policy enables program controllable function to smartly choose ideal anisotropic field based on the grain boundary orientation information reported to the program to relax grain boundary at its best extent.

In the work we report above, grain boundary can be relaxed through four methods, including constant electric field by solely itself, periodic relaxation of ensemble, non-determined and determined morphology change between isotropic and anisotropic electric field. Among them, the close loop anisotropic policy shows its superior behavior on relaxing grain boundary, obtaining defect free perfect crystal structure in high yield and short time cost. The simulation and experimental results are consistent and prove the feasibility of control policies designed. More than that, we also empirically optimized update time from 50s to 20s to further shorten the time cost for assembly, and results show significant lower time cost while maintaining a high yield of perfect crystal.

The work we reported here exhibits great improvement on colloid assembly experiment, provides new method on producing big single domain colloid crystals in high efficiency and in short time through anisotropic electric field generated by newly designed octupole electrodes, with the help of open-loop and closed-loop policies.

5.2 Future Work

There are many factors influence the efficient colloid assembly process. Several factors can be modified through the experiment to improve performance of colloid assembly, including the image analysis algorithm, feedback control algorithm, and even inventing new control policy. We aim to maintain the high yield of perfect crystal, and shorten time cost as low as possible.

As stated in previous sections, the image analysis function is flawed by the image noise, video capture error and particle tracking error. We can try to develop new MATLAB command to exclude these errors from analysis.

Also, we notice some of the perfect crystal obtained in experiments exhibits oval shape, however, the crystal structure is defined as a single big domain of circular structure. We can try to apply isotropic electric field to quench colloid array into circular structure after it nearly reach the perfect crystal state. The duration for applying isotropic electric field can also be determined by using close loop, if we introduce the ensemble anisotropy as another parameter feedbacked to the system, and based on that, program automatically choose the duration of isotropic field applied. The simulation of this process shows feasibility on doing it, almost all cycles achieve circular shape without losing its perfect crystal structure.

Furthermore, previous cycles of experiments always start with fluid phase condition with particles randomly distributed above the surface. Under this situation, most cycles reach a high ψ_6 value at its initial ensemble and makes the whole process easy to finish. We aim to make the problem we want to solve much difficult, so we propose to start

our new cycles of experiment at condense phase with ψ_6 value lower than 0.6. Control policies stated in this report will be executed under new initial condition to examine its efficiency. New policies will also be developed to tune colloid assembly process better.

REFERENCES

1. Genovese, D. B.; Lozano, J. E.; Rao, M. A., The rheology of colloidal and noncolloidal food dispersions. *J Food Sci* **2007,** *72* (2), R11-20.

2. Hosein, I. D.; Liddell, C. M., Homogeneous, core-shell, and hollow-shell ZnS colloid-based photonic crystals. *Langmuir* **2007,** *23* (5), 2892-7.

3. Peymannia, M.; Soleimani-Gorgani, A.; Ghahari, M.; Najafi, F., Production of a stable and homogeneous colloid dispersion of nano CoAl2O4 pigment for ceramic ink-jet ink. *Journal of the European Ceramic Society* **2014,** *34* (12), 3119-3126.

4. Pouton, C. W., Formulation of self-emulsifying drug delivery systems. *Advanced Drug Delivery Reviews* **1997,** *25* (1), 47-58.

5. Xenakis, A.; Papadimitriou, V.; Sotiroudis, T. G., Colloidal structures in natural oils. *Current Opinion in Colloid & Interface Science* **2010,** *15* (1-2), 55-60.

6. Mason, T. G.; Bibette, J.; Weitz, D. A., Yielding and Flow of Monodisperse Emulsions. *Journal of Colloid and Interface Science* **1996,** *179* (2), 439-448.

7. Subramanian, G.; Manoharan, V. N.; Thorne, J. D.; Pine, D. J., Ordered Macroporous Materials by Colloidal Assembly: A Possible Route to Photonic Bandgap Materials. *Advanced Materials* **1999,** *11* (15), 1261-1265.

8. Stratford, K.; Henrich, O.; Lintuvuori, J. S.; Cates, M. E.; Marenduzzo, D., Self-assembly of colloid-cholesteric composites provides a possible route to switchable optical materials. *Nature Communications* **2014,** *5* (1).

9. Velev, O. D.; Kaler, E. W., Structured Porous Materials via Colloidal Crystal Templating: From Inorganic Oxides to Metals. *Advanced Materials* **2000,** *12* (7), 531-534.

10. Wang, Y.; Wei, G.; Wen, F.; Zhang, X.; Zhang, W.; Shi, L., Synthesis of gold nanoparticles stabilized with poly(N-isopropylacrylamide)-co-poly(4-vinyl pyridine) colloid and their application in responsive catalysis. *Journal of Molecular Catalysis A: Chemical* **2008,** *280* (1-2), 1-6.

11. Wang, D.; Möhwald, H., Template-directed colloidal self-assembly – the route to 'top-down' nanochemical engineering. *J. Mater. Chem.* **2004,** *14* (4), 459-468.

12. Nam, H. J.; Kim, J.-H.; Jung, D.-Y.; Park, J. B.; Lee, H. S., Two-dimensional nanopatterning by PDMS relief structures of polymeric colloidal crystals. *Applied Surface Science* **2008,** *254* (16), 5134-5140.

13. Brinker, C. J.; Lu, Y.; Sellinger, A.; Fan, H., Evaporation-Induced Self-Assembly: Nanostructures Made Easy. *Advanced Materials* **1999,** *11* (7), 579-585.

14. Liu, G.; Shao, J.; Zhang, Y.; Wu, Y.; Wang, C.; Fan, Q.; Zhou, L., Self-assembly behavior of polystyrene/methacrylic acid (P(St-MAA)) colloidal microspheres on polyester fabrics by gravitational sedimentation. *The Journal of The Textile Institute* **2015,** *106* (12), 1293-1305.

15. Baranov, D.; Fiore, A.; van Huis, M.; Giannini, C.; Falqui, A.; Lafont, U.; Zandbergen, H.; Zanella, M.; Cingolani, R.; Manna, L., Assembly of colloidal semiconductor nanorods in solution by depletion attraction. *Nano Lett* **2010,** *10* (2), 743-9.

16. Sahoo, Y.; Cheon, M.; Wang, S.; Luo, H.; Furlani, E. P.; Prasad, P. N., Field-Directed Self-Assembly of Magnetic Nanoparticles. *The Journal of Physical Chemistry B* **2004,** *108* (11), 3380-3383.

17. Dreher, M. R.; Simnick, A. J.; Fischer, K.; Smith, R. J.; Patel, A.; Schmidt, M.; Chilkoti, A., Temperature triggered self-assembly of polypeptides into multivalent spherical micelles. *J Am Chem Soc* **2008,** *130* (2), 687-94.

18. Whitesides, G. M.; Grzybowski, B., Self-assembly at all scales. *Science* **2002,** *295* (5564), 2418-21.

19. Mirkin, C. A.; Letsinger, R. L.; Mucic, R. C.; Storhoff, J. J., A DNA-based method for rationally assembling nanoparticles into macroscopic materials. *Nature* **1996,** *382* (6592), 607-609.

20. Velev, O. D.; Kaler, E. W., In situ assembly of colloidal particles into miniaturized biosensors. *Langmuir* **1999,** *15* (11), 3693-3698.

21. Lu, C.; Möhwald, H.; Fery, A., A lithography-free method for directed colloidal crystal assembly based on wrinkling. *Soft Matter* **2007,** *3* (12), 1530.

22. Hayward, R. C.; Saville, D. A.; Aksay, I. A., Electrophoretic assembly of colloidal crystals with optically tunable micropatterns. *Nature* **2000,** *404* (6773), 56-9.

23. Yeh, S. R.; Seul, M.; Shraiman, B. I., Assembly of ordered colloidal aggregrates by electric-field-induced fluid flow. *Nature* **1997,** *386* (6620), 57-59.

24. Velev, O. D.; Bhatt, K. H., On-chip micromanipulation and assembly of colloidal particles by electric fields. *Soft Matter* **2006,** *2* (9), 738.

25. Juarez, J. J.; Bevan, M. A., Interactions and microstructures in electric field mediated colloidal assembly. *J Chem Phys* **2009,** *131* (13), 134704.

26. Tang, X.; Rupp, B.; Yang, Y.; Edwards, T. D.; Grover, M. A.; Bevan, M. A., Optimal Feedback Controlled Assembly of Perfect Crystals. *ACS Nano* **2016,** *10* (7), 6791-8.

27. Ma, F.; Wang, S.; Wu, D. T.; Wu, N., Electric-field-induced assembly and propulsion of chiral colloidal clusters. *Proc Natl Acad Sci U S A* **2015,** *112* (20), 6307-12.

28. Yan, J.; Bloom, M.; Bae, S. C.; Luijten, E.; Granick, S., Linking synchronization to self-assembly using magnetic Janus colloids. *Nature* **2012,** *491* (7425), 578-+.

29. Donath, E.; Sukhorukov, G. B.; Caruso, F.; Davis, S. A.; Mohwald, H., Novel Hollow Polymer Shells by Colloid-Templated Assembly of Polyelectrolytes. *Angew Chem Int Ed Engl* **1998,** *37* (16), 2201-2205.

30. Meijer, J. M.; Hagemans, F.; Rossi, L.; Byelov, D. V.; Castillo, S. I.; Snigirev, A.; Snigireva, I.; Philipse, A. P.; Petukhov, A. V., Self-assembly of colloidal cubes via vertical deposition. *Langmuir* **2012,** *28* (20), 7631-8.

31. Gong, T. Y.; Wu, D. T.; Marr, D. W. M., Electric field-reversible three-dimensional colloidal crystals. *Langmuir* **2003,** *19* (15), 5967-5970.

32. Juarez, J. J.; Feicht, S. E.; Bevan, M. A., Electric field mediated assembly of three dimensional equilibrium colloidal crystals. *Soft Matter* **2012,** *8* (1), 94-103.

33. Lee, J. H.; Wu, Q.; Park, W., Metal nanocluster metamaterial fabricated by the colloidal self-assembly. *Opt Lett* **2009,** *34* (4), 443-5.

34. Edwards, T. D.; Beltran-Villegas, D. J.; Bevan, M. A., Size dependent thermodynamics and kinetics in electric field mediated colloidal crystal assembly. *Soft Matter* **2013,** *9* (38), 9208-9218.

35. Juarez, J. J.; Cui, J. Q.; Liu, B. G.; Bevan, M. A., kT-scale colloidal interactions in high frequency inhomogeneous AC electric fields. I. Single particles. *Langmuir* **2011,** *27* (15), 9211-8.

36. Bevan, M. A.; Prieve, D. C., Direct measurement of retarded van der Waals attraction. *Langmuir* **1999,** *15* (23), 7925-7936.

37. Hunter, R. J., Zeta potential in colloid science : principles and applications. **1981**.

38. Gast, A. P.; Zukoski, C. F., Electrorheological fluids as colloidal suspensions. *Advances in Colloid and Interface Science* **1989,** *30*, 153-202.

39. Saville, D. A.; Bellini, T.; Degiorgio, V.; Mantegazza, F., An extended Maxwell-Wagner theory for the electric birefringence of charged colloids. *J Chem Phys* **2000,** *113* (16), 6974-6983.

40. Jones, T. B.; Washizu, M., Equilibria and Dynamics of Dep-Levitated Particles - Multipolar Theory. *J Electrostat* **1994,** *33* (2), 199-212.

41. Fernandes, G. E.; Beltran-Villegas, D. J.; Bevan, M. A., Interfacial colloidal crystallization via tunable hydrogel depletants. *Langmuir* **2008,** *24* (19), 10776-85.

42. Fernandes, G. E.; Beltran-Villegas, D. J.; Bevan, M. A., Spatially controlled reversible colloidal self-assembly. *J Chem Phys* **2009,** *131* (13), 134705.

43. Halperin, D. R. N. a. B. I., Dislocation-mediated melting in two dimensions. *Phys. Rev. B 19*.

44. P. R. ten Wolde, M. J. R.-M. a. D. F., *The Journal of Chemical Physics 104 (24)*.

45. tenWolde, P. R.; RuizMontero, M. J.; Frenkel, D., Numerical calculation of the rate of crystal nucleation in a Lennard-Jones system at moderate undercooling. *J Chem Phys* **1996,** *104* (24), 9932-9947.

VITA

Name: Junyan Yang

Birth: April, 10, 1995, Tianjin, China

Address: Junyan Yang may be contacted through Dr. M. A. Bevan at the Chemical and Biomolecular Engineering Department, Johns Hopkins University, Baltimore, MD, 21218

Email: jyang146@jhu.edu

Education: B.E., Tianjin University, 2017, China

Research: Synthesis of Nano-sized photo-responsive catalyst induced by amino acids
With Dr. T. Zhang, Tianjin University, 2016-2017